Metals and Materials International (2023) 29:1–17
https://doi.org/10.1007/s12540-022-01222-8

Anti-Corrosion Coatings for Protecting Nb-Based Alloys Exposed to Oxidation Environments: A Review

Yingyi Zhang[1] · Tao Fu[1] · Laihao Yu[1] · Kunkun Cui[1] · Jie Wang[1] · Fuqiang Shen[1] · Xu Zhang[1] · Kaichuang Zhou[2]

Received: 11 February 2022 / Accepted: 8 April 2022 / Published online: 3 June 2022

Abstract
Nb-based alloys are regarded as a vital high temperature structural material. Unfortunately, the low oxidation resistance of the alloys limits their application under aerobic conditions at high temperature. Surface coating technology is considered to be an ideal method to solve this problem. This paper reviewed recent progress on silicide coatings on Nb and Nb-based alloy, and focused on different types of modification techniques. The microstructure, phase composition and oxidation properties of various silicified coatings are analyzed. The effects of modified elements and second phase on the oxidation mechanism of silicide coatings are also summarized. Finally, the existing problems and future development direction of various silicide coatings are pointed out.

Keywords Nb-based alloys · Coatings · Oxidation behavior · Microstructure · Mechanism

1 Introduction

Nb-based alloys have a good toughness, high melting point, good electrical and thermal conductivity and sufficient high temperature strength. Therefore, they are widely used in superconducting materials, aerospace, atomic energy, electronics and other industrial fields [1–4]. However, the low oxidation resistance of the alloys prevents their long-term use in high temperature aerobic environments [5, 6]. At present, the alloying method and surface coating technology are two main methods to solve this problem [7, 8]. The oxidation resistance of Nb can be improved partly by addition of silicon, and Nb-Si based alloys have good mechanical properties [9]. Unfortunately, this is not sufficient to solve the problem of poor oxidation resistance of the alloys [9, 10]. This is because the alloys will be oxidized to form unprotected porous Nb_2O_5 and NbO_2 oxides under high temperatures aerobic conditions, which does not prevent further oxidation of the alloys [11–15]. In addition, adding appropriate amount of Al, Ti, Cr, Hf and other elements to Nb-Si based alloys is also beneficial to improve their oxidation resistance [16, 17]. Among them, Hf and Ti can reduce the growth stress of oxides and maintain the integrity of the oxide layer [18]. Al and Cr are good to reduce the diffusion rate of Nb_{ss} and slow down the oxidation of the alloy [19]. However, improper elemental ratio will make the mechanical properties of the alloys unsatisfactory. With the increase of Cr content from 2 to 17%(at%), the room-temperature toughness of Nb-Si based alloys drop to 8.5 MPa·$m^{1/2}$ from 14.5 MPa·$m^{1/2}$ [20, 21]. Therefore, the result of alloying is not satisfactory when the mechanical properties and high-temperature oxidation resistance of the alloys taken both into consideration at the same time. Related scholars have realized that surface coating technology is an ideal method to overcome this problem [22, 23]. The researches shows that the silicified coatings have good thermal stability and their operating temperature can reach 1600 °C. The SiO_2 protective film formed on the surface of coating can act as a diffusion barrier to prevent the diffusion of oxygen into the substrate. In addition, the viscosity of SiO_2 at high temperature is low, and its fluidity is enhanced, which makes the coatings have a certain self-healing and resisting deformation ability [24–26]. Moreover, the high-temperature oxidation resistance of the coatings can be further improved with the addition of modified elements and the introduction of second phases. Among them, the addition of Al, B, W, Y, Re, Ge, Ce, Y_2O_3 and aluminum silicate (mullite) are the most common [27–29].

✉ Yingyi Zhang
zhangyingyi@cqu.edu.cn

[1] School of Metallurgical Engineering, Anhui University of Technology, Maanshan 243002, Anhui Province, China

[2] School of Mechanical Engineering, Anhui University of Technology, Maanshan 243002, Anhui Province, China

At present, there are many reports on the application of surface coating technology in the oxidation protection of Nb and its alloys [30]. This paper summarizes the researches of domestic and foreign scholars in this field for many years. In this work, the microstructure, phase composition, oxidation behavior and failure mechanism of various silicified coatings on Nb-based alloys are analyzed and summarized, comprehensively. The main silicified coatings are divided into four categories: single silicified coating, composite silicified coating, single element modified silicified coating and composite element modified silicified coating. The effects of the addition of various modified elements on the oxidation behavior of coatings are summarized in depth, and the specific measures improving the oxidation resistance of coatings at high temperature are pointed out.

2 Microstructure and Oxidation Properties of Silicide Coatings

2.1 Single Silicide Coating

2.1.1 Microstructure and Phase Composition of the Coatings

Single silicide coating is formed by interdiffusion between silicon element and substrate and metallurgical bonding, which has a single composition and structure [31, 32]. Halide activated pack cementation(HAPC), a significant surface coating preparation technology, is favored by researchers because of its wide source of raw materials, strong operability, uniform composition of the coating prepared, compact structure and good combination with the substrate. The principle of this process is to mix the donor sources (Si, B, Al, SiC powder, etc.), inert filler (Al_2O_3 powder) and halide activator (NH_4Cl/Na, NaF, etc.) in a certain proportion evenly, put them into the corundum crucible. Then the substrate is embedded into the mixture, through inert gas and covered with Al_2O_3 plate. The crucible is placed into the furnace, and at high temperature, the donor source in the mixture will be deposited to the substrate surface by thermal diffusion to form a coating, as shown in Fig. 1 [33].

Vishwanadh et al. [34] prepared the $NbSi_2$ coating by halide activated pack cementation (HAPC) at different temperatures, successfully, as shown in Fig. 1. It is observed that the surface of the coatings are composed of uniform silicified particles, and the particle size increases gradually with increasing temperature. This is caused by the recrystallization of $NbSi_2$ particles in the deposition process, as shown in Fig. 2a–d. In addition, the interdiffusion between Si and Nb enhance gradually with increasing temperature, making the thicknesses of $NbSi_2$ and Nb_5Si_3 layers increase significantly, as shown in Fig. 2e–h. Although a few microcracks are observed on the surface of sample at 1200 °C, but the interior of the sample is very dense, and a thin Nb_5Si_3 layer forms between the coating and substrate, as shown in Fig. 2a and e. Similar results are also observed in the sample deposited at 1300 °C, as shown in Fig. 2b and f. Moreover, when the temperature is 1400 °C, a mass of pores appear both on the surface and inside of the sample. This is because the temperature is close to the melting point of Si (1410 °C), which makes the precipitated Si particles melt soft, resulting in the formation of pores between $NbSi_2$ particles, as shown in Fig. 2c and g [35]. It is worth noting that when the deposition temperature reaches 1500 °C, the coating has a smooth and dense surface, and there are white pure Si precipitates in local areas. However, obvious cracks were observed inside the coating, which is related to the mismatch of the thermal expansion coefficient (CTE) between the coating and substrate, as shown in Fig. 2d and h.

Liu et al. [36] produced $MoSi_2$ coating on surface of the Nb-10Hf-1Ti alloy by two-step deposition process. It can be seen that the coating has a rough surface with some cracks and holes. Similar phenomena also be

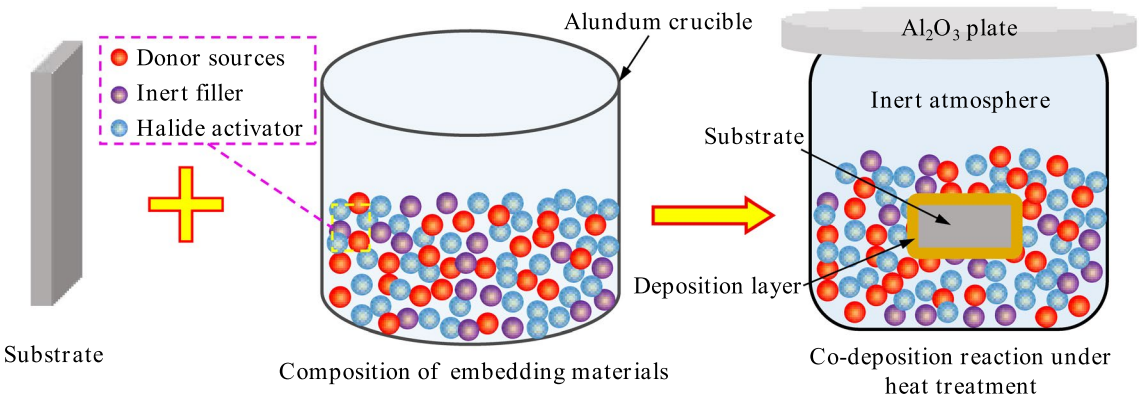

Fig. 1 Schematic diagram of the co-deposition reaction model of the HAPC method

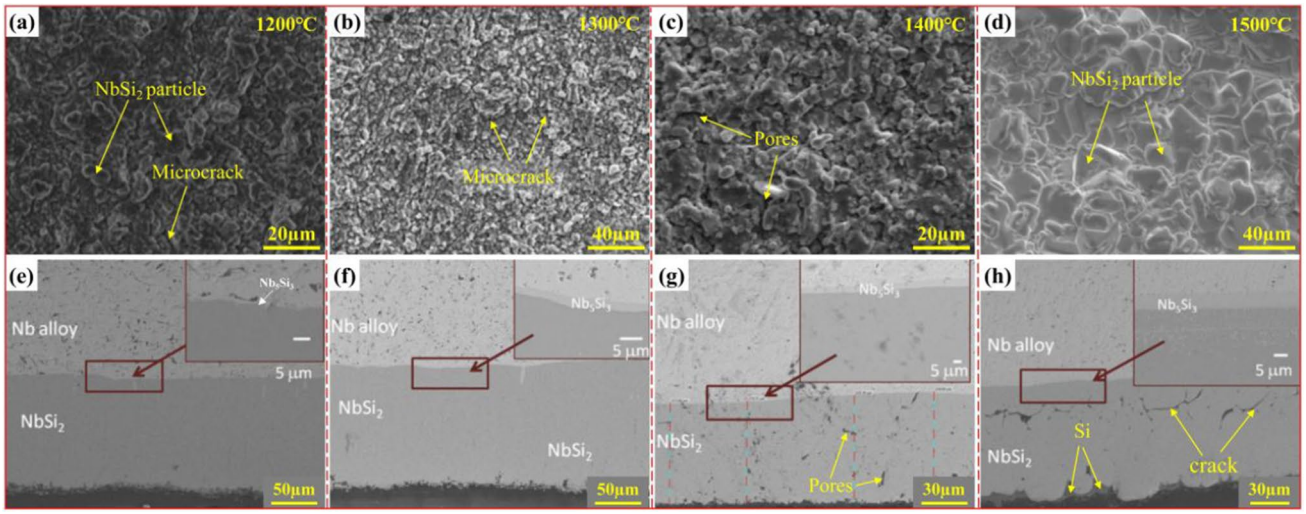

Fig. 2 The images of surface and corresponding cross-section of the $NbSi_2$ coatings were obtained on the surface of Nb-1Zr-0.1C alloy by deposited at different temperatures for 6 h [34]

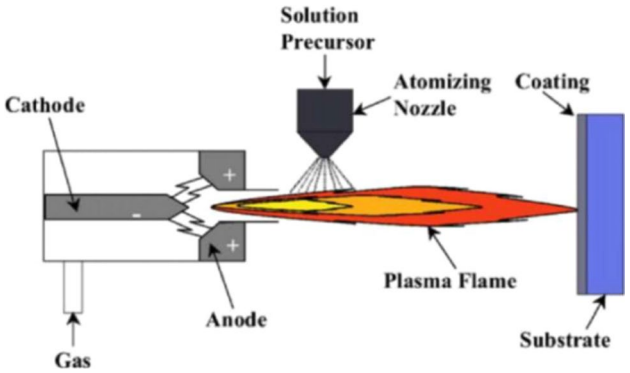

Fig. 3 Schematic diagram of the SAPS process principle [38]

observed between the $MoSi_2$ layer and bond layer inside of the coating, as shown in Fig. 3a and b, respectively. The mismatch of CTE between $MoSi_2$ (8.0×10^{-6}/°C) and substrate ($7.8–8.2 \times 10^{-6}$/°C) is the main reason for this result [37]. As an important surface engineering technology, supersonic plasma spraying technology(SAPS) has the advantages of high deposition efficiency, low energy consumption, low cost and good coating quality. Its principle is to take the plasma arc as the heat source, the working gas (N_2, H_2, Ar, He, etc.) is heated to form high temperature and high speed plasma jet (the temperature can reach tens of thousands of degrees Celsius). The plasma jet can heat the spraying material to molten and semi-molten states, and spray it to the substrate surface at high speed to form coating, as shown in Fig. 3 [38].

Sun et al. [39] reported the $MoSi_2$ coating obtained by SAPS technology. The surface of the coating is composed of molten and semi-molten particles with poor uniformity and a large number of pores. This is caused by the melting and recrystallization of the spraying material on the coating surface [40, 41]. In addition, some areas of the coating surface oxidized because of the high spraying temperature and the fact that the whole process took place in air. The tests result of XRD shows that both points A and B contain a small quantity of SiO_2, as shown in Fig. 4c. While the interior of the coating is relatively dense and the overall thickness is about 200 μm, as shown in Fig. 4d.

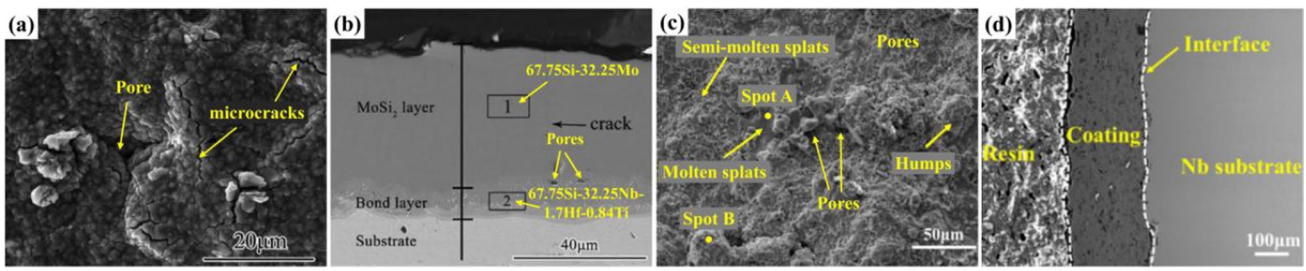

Fig. 4 Typical surface and corresponding section morphology of $MoSi_2$ coatings on Nb-based alloys and Nb; **a** and **b** [36], **c** and **d** [39]

2.1.2 Oxidation Properties of the Coatings

Choi et al. [42] researched the oxidation behavior of $NbSi_2$ coatings at different temperatures. The results show that oxidized coatings are composed of an oxide layer, a $NbSi_2$ layer and an interface layer, respectively. In the temperature range of 1000 °C to 1200 °C, some cracks were observed inside the coatings, the thickness and the porosity of the oxide layer increase significantly with the increase of temperature, as shown in Fig. 5a–c. However, the coating has a maximum Δm/S, a thickest oxide layer and a highest porosity at the deposition temperature of 1300 °C, as shown in Fig. 5d. Moreover, a mass of white oxide particles were observed at the sample appearance, as shown in Fig. 6. The authors believe that the volatile NbO_2 produced by the decomposition of Nb_2O_5 during oxidation is the main reason for this result [43]. When the temperature is between 1400 and 1450 °C, the oxide layer of the coatings becomes thinner and tends to be smooth, as shown in Fig. 5e and f. This is attributed to that the *c*-SiO_2 with a high density and certain fluidity is generated, which is spreading along the coating surface and filling up the pores in the oxide layer. It should be noted that the thickness of the interfacial layer (Nb_5Si_3 layer) increases gradually with increasing temperature because of the principle of thermal diffusion. Overall, the oxidation of the coating is complex and does not show a simple dependence on temperature. The quality of the oxide layer, the stability of the structure and the self-healing ability of the coating all have important effects on its oxidation behavior at different temperatures.

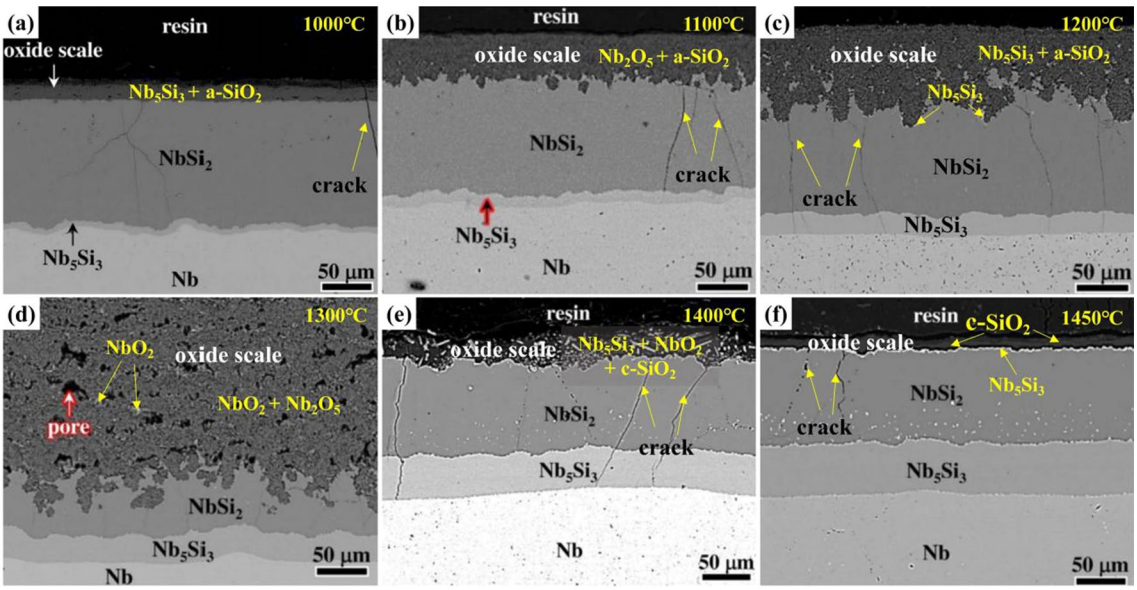

Fig. 5 The images of cross-sectional of the oxidized $NbSi_2$ coating observed for 50 h at different temperatures [41]

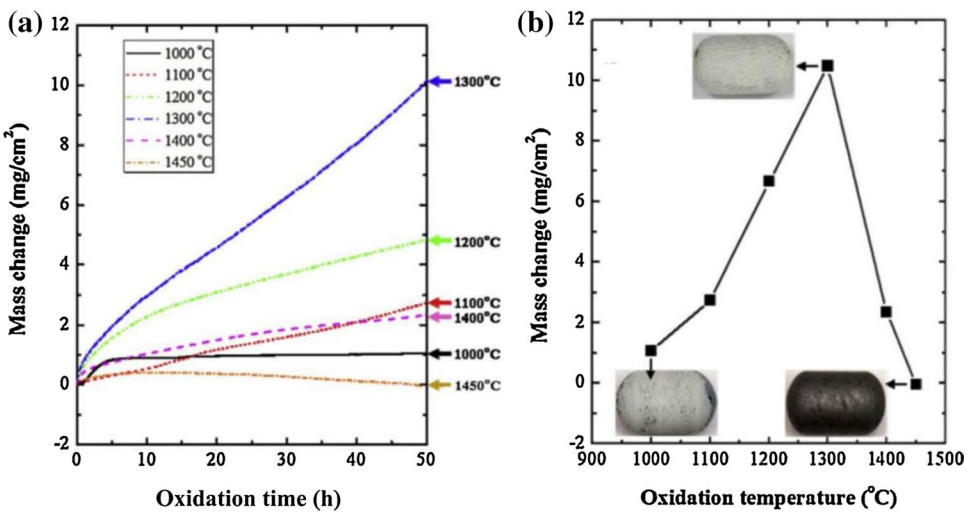

Fig. 6 The Δm/S of $NbSi_2$ coatings varies with time **a** and the appearance of the coatings varies with temperature **b** at the oxidation atmosphere of 1000–1450 °C [42]

The pictures of the oxidized $MoSi_2$ coating on the Nb-5 W-2.2Mo-1.6Zr(wt%) alloy are shown in Fig. 7 [39]. The results show oxidized coating has a more smooth and even surface, which is composed of black particles (Mo_5Si_3) and gray glassy film (SiO_2), respectively. However, due to the differences in CTE between Mo_5Si_3 and SiO_2, some microscopic cracks are still observed on the surface of the coating, as shown in Fig. 7a. The oxide layer is mainly composed of SiO_2, which shows continuous inhomogeneity because of the high surface roughness of coating. At the same time, SiO_2 has good fluidity at high temperature, which is improves the self-healing ability of the coating to some extent, as shown in Fig. 7b [44]. The interior of the coating is mainly composed of $MoSi_2$, Mo_5Si_3 and SiO_2, and contains a large number of pores. Which is caused by the decomposition of $MoSi_2$ and the generation and volatilization of MoO_3, as shown in Fig. 7c. Liu et al. [37] reported that the $MoSi_2$ coating can provide effective protection for Nb-10Hf-1Ti alloy for a long time at the temperature of 1200 °C. After 100 h of oxidation, the coated sample still maintained its intact structure, and its mass gain was only 0.64 mg cm^{-2}. However, the bare alloy was completely "powdered" after oxidation for 10 h, as shown in Fig. 8a. The fitting results of oxidation kinetics curves of coating samples show that the process follows a parabolic rule [45]. According to the relevant formula, the oxidation rate kp of the coating is only 1.69×10^{-4} $mg^2 \cdot cm^{-4} \cdot h^{-1}$, as shown in Fig. 8b [46].

2.2 Composite Silicide Coatings

2.2.1 Microstructure and Phase Composition of Coatings

Composite silicide coating is a kind of coatings obtained through the organic combination of a single silicide coating, and its structure has been further optimized compared with the single silicide coating [47–49]. The surface and corresponding cross-section morphologies of typical composite silicide coatings are shown in Fig. 9. Yue et al. [50] prepared the $MoSi_2$-$Resi_2$-$NbSi_2$ coating by HAPC method. XRD results show that there are a lot of SiO_2 and Al_2O_3 particles on the coating surface besides $MoSi_2$. This means that the original oxide layer formed on the coating surface during the HAPC process [51]. In addition, a few microcracks were also observed on its surface, as shown in Fig. 9a.

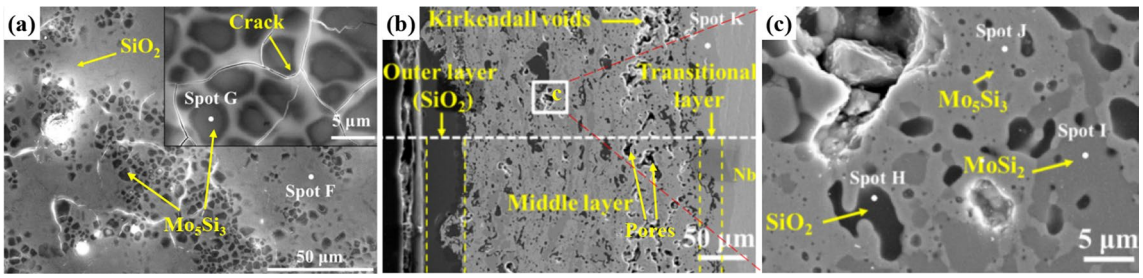

Fig. 7 Surface **a** and corresponding cross-section **b** of $MoSi_2$ coating after oxidation at 1500 °C for 43 h, **c** is detail of the middle layer corresponding to the white rectangle in **b** [39]

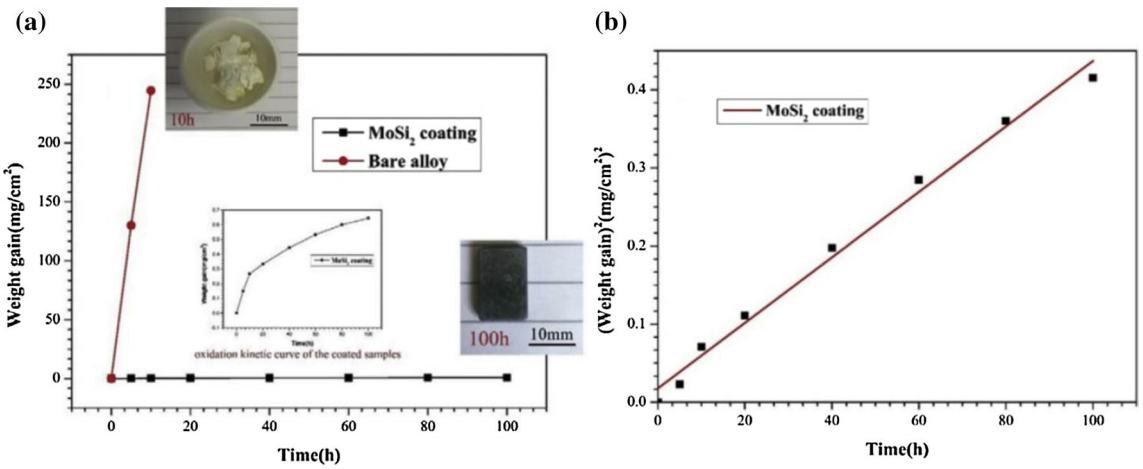

Fig. 8 The Δm/S **a** and $(\Delta m/S)^2$ **b** of $MoSi_2$ coating varies with time at oxidation tests at 1200 °C for 100 h [37]

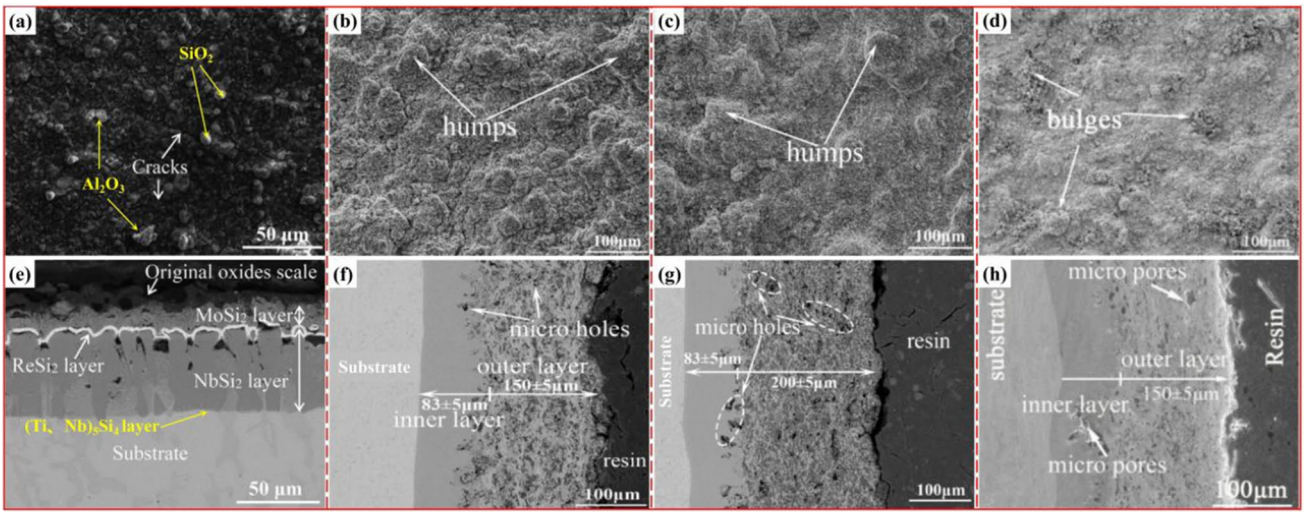

Fig. 9 The BSE images of surface and corresponding cross-sectional of the various coatings on niobium and its alloy; $MoSi_2/ReSi_2/NbSi_2$ coating **a** and **e** [49], M10 coating **b** and **f**, M30 coating **c** and **g** [51], WMM coating **d** and **h** [53]

However, the inner of coating is relatively dense, composed of $MoSi_2$, $ReSi_2$ and $NbSi_2$ layers from outside to inside. Moreover, there is a thin $(Ti,Nb)_5Si_4$ transition layer between the $NbSi_2$ layer and substrate, as shown in Fig. 9e. Zhang et al. [52] prepared 10 wt% and 30 wt% mullite $MoSi_2$ coatings (MM), respectively, on the surface of Nb521 alloy by HAPC and SAPS techniques. Although the surface of coatings was relatively rough, no obvious cracks, holes and other defects were found, as shown in Fig. 9b and c. This is due to the melted mullite filled up the pores on the coating surface during the injection process. The inner coatings was very dense and tightly bonded to the substrate, as shown in Fig. 9f and g, respectively. Notably, many pores and unfused loose particles are observed in the M30 coating. This is related to the insufficient melting of $MoSi_2$ due to the high content of mullite in the sample and its relatively low melting point, as shown in Fig. 9g. In addition, Zhang et al. [53] also studied the WSi_2-Mullite-$MoSi_2$ (WMM) composite coating on Nb surface. Compared with MM coating, the surface of the WMM coating was more uniform, the particles were finer, and the typical lamellar structure was presented. The interior of the coating was more dense and its porosity was reduced significantly, as shown in Fig. 9d and h.

2.2.2 Oxidation Properties of the Coatings

The images of the oxidized composite silicide coatings are shown in Fig. 10. It can be seen that the surfaces of $MoSi_2/ReSi_2/NbSi_2$, M10 and WMM coatings are smooth and compact, with a uniform oxide film, as shown in Fig. 10a, b and d [50, 52, 53]. Unfortunately, a mass of micro-pores were observed in the lamellar Nb_2O_5 on the surface of MM coating, which may be related to the volatilization of MoO_3 and SiO_2[54], as shown in Fig. 10c. In addition, many cracks and holes appeared inside the MM coating, and serious exfoliation of the interface layer was observed, and the protective oxide film almost completely disappeared, as shown in Fig. 10g. But, for oxidized $MoSi_2/ReSi_2/NbSi_2$ coating, a thin $MoSi_2/ReSi_2$ layer was still observed at the bottom of the oxide layer of the coating, as shown in Fig. 10e. This shows that the $ReSi_2$ layer improves the adhesion of $MoSi_2$ layer, limits the diffusion of Si, and enhances the oxidation resistance of the coating [55].

Zhang et al. [53] studied the effects of the addition of mullite and WSi_2 on the oxidation properties of $MoSi_2$ coating. The results show that the $\Delta m/S$ of M0 and M30 samples changed significantly after oxidation for 118 h and 30 h. Among them, the oxide layer on the surface of sample M30 darkened and decomposed, and the sample M0 was pulverized completely. However, after 70 h of oxidation, the surface of M10 sample is very smooth and the mass change is quite stable, only $-4.06\ mg{\cdot}cm^{-2}$, as shown in Fig. 11a. Even after 140 h of oxidation, it still shows stable oxidation resistance, with a smooth and dense surface and a thin and uniform oxide layer, as shown in Fig. 10b and f. Compared with the single $MoSi_2$ coating, more amorphous SiO_2 was detected on the surface of MM sample, which means that the addition of mullite inhibited the crystallization of SiO_2 and improved its fluidity at high temperature [54]. What is noteworthy is that the mass loss of the WMM coating was only $4.41\ mg{\cdot}cm^{-2}$ after 500 h of oxidation, as shown in Fig. 11b. The test results show that solid solution phases of (Mo,W)Si_2 with the CTE similar to that of SiO_2 are formed on the coating surface, as shown in Fig. 10d. Which is effectively alleviating defects caused by CTE mismatch on the surface of the coating [56–58]. The oxidized coating was composed

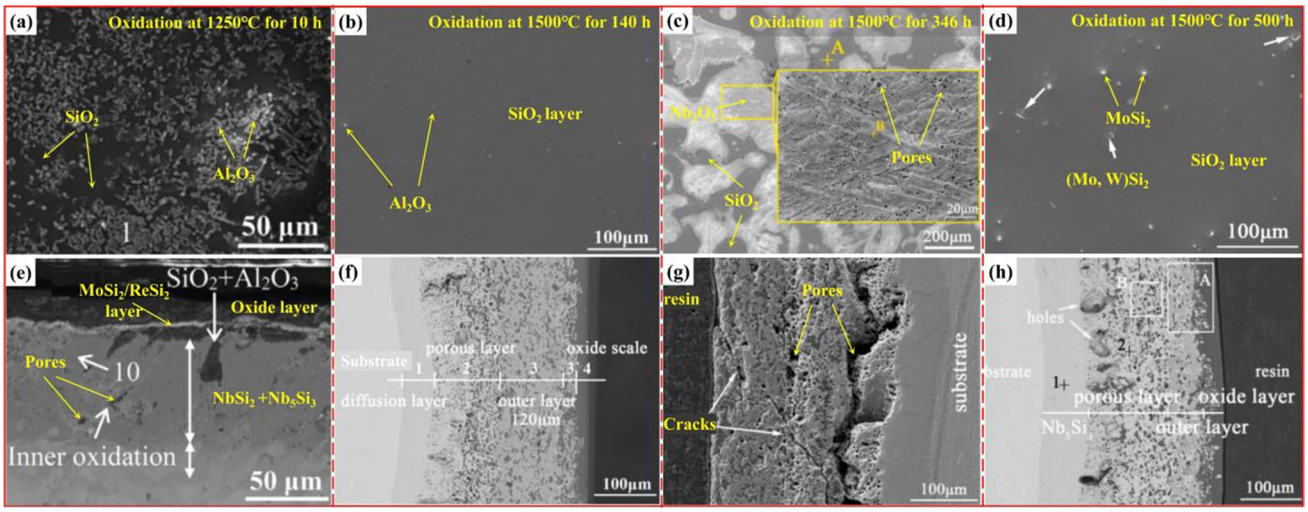

Fig. 10 The oxidized surface and corresponding cross-sections of various composite silicified coatings on Nb and Nb-based alloys under different conditions; $MoSi_2/ReSi_2/NbSi_2$ coating **a** and **e** [50], M10 coating **b** and **f**, MM coating **c** and **g** [52], WMM coating **d** and **h** [53]

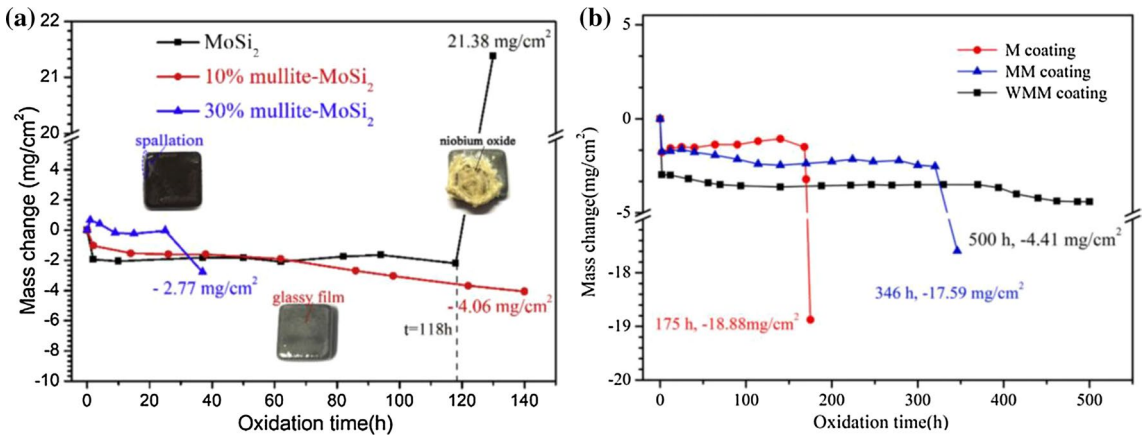

Fig. 11 Oxidation kinetics curves and corresponding appearance pictures of different coatings at 1500 °C [53]

of the oxide layer, outer layer, porous layer and interface layer. The results of chemical composition detection in typical regions of each layer showed that its main components were SiO_2, $(Mo,W)Si_2$, $(Mo,W)_5Si_3$, $(Mo,W,Nb)_5Si_3$ and Nb_5Si_3, respectively, as shown in Fig. 10h. This means that the WSi_2 inhibits the diffusion of Si element, maintains the structure of coating, and ensures the oxidation service life of coating at high temperature [59].

3 Microstructure and oxidation behavior of modified silicide coatings

Adding appropriate amount of modified elements to the silicified coating is a vital way to enhance the high-temperature oxidation resistance of coating. Among them, the researches of Al, B, Y, Re, Ge, Ce and other elements to improve the oxidation properties of Nb and its alloy surface silicide coating have been favored by relevant scholars.

3.1 Silicide Coating Modified by Single Element

3.1.1 Microstructure and Phase Composition of the Coatings

Wang et al. [60] produced the Ge-modified silicide coating by HAPC method. The interior of the coating has uniform composition, dense structure, and a few cracks. The results of XRD and EDS analysis show that the main components of inner and outer layers are $(Nb,X)_5(Si,Ge)_3$ and $(Nb,X)(Si,Ge)_2$(X represents Ti, Cr, Hf elements), and their thicknesses are 11 μm and 165 μm, respectively, as shown

in Fig. 12a. This indicates that during diffusing into the substrate, the concentration of Nb, Ti and other elements increases gradually, while the Si element decreases gradually. In addition, due to the phase with higher Nb content has a larger lattice constant, higher Ge content is detected in the diffusion layer [61–63], as shown in Fig. 12e. Qiao et al. [64] prepared the Y-modified silicide coating by Si-Y co-deposition technology. EDS test results show that the coating is composed of light gray (Nb,Cr) Si_2 and dark gray (Cr,Nb) Si_2, with an overall thickness of more than 200 μm, as shown in Fig. 12b. Noteworthy, there is no obvious change in Si concentration distribution throughout the coating, and the content of Y element on the outer side of coating is slightly higher than that on the inner side, as shown in Fig. 12f. However, the Mo-Si-Al coating has an obvious layered structure, which consists of a dark gray outermost layer, a gray and white inter layer and a light gray inner layer. The analysis results of the components of each layers show that the outer layer is $Mo(Si,Al)_2$ rich layer, the middle layer is $Mo_5(Si,Al)_2$ and Al_8Mo_3 rich layer, and the inner layer is $AlMo_3$ rich layer, as shown in Fig. 12c and g [65], respectively. The Mo-Si-B coating has a relatively uniform and dense surface, which is main components are $MoSi_2$ and B_2O_3-SiO_2, as shown in Fig. 12d [66]. This is due to the presence of a small amount of oxygen in the system during the preparation of coating, resulting in the oxidation of local areas on the surface of coating. The results of WDS analysis show that there is an obvious layered structure inside the coating, and the B element is mainly distributed in the intermediate layer composed of $(Nb,Ti)_5SiB_2$, as shown in Fig. 12h. Which means that the solubility of B in $MoSi_2$ (outer layer) and (Nb,Ti) Si_2 (inner layer) is low [67].

3.1.2 Oxidation Properties of the Coatings

The images of the oxidized silicide coatings modified by single element are shown in Fig. 13. It is observed that the surface of the oxidized Mo-Si-Al coating is covered with a shiny particles layer, and its main ingredients are a-Al_2O_3 and $Mo_5(Si,Al)_3$, as shown in Fig. 13a [65]. In addition, many pores were observed in the $Mo_5(Si,Al)_3$ layer, which may be related to the production of volatile MoO_3. However, the internal structure of the coating remained intact and tightly bonded to the substrate, as shown in Fig. 13e. The selective oxidation of Al element promoted the formation of protective oxide film on the surface of the coating, prolonged the oxidation service life of the coating, as reported in the study of Majumdar [68, 69]. The results of EDS and XRD test show that a compact B_2O_3-SiO_2 layer formed on the surface of the oxidized Mo-Si-B coating, and the diffraction peak of Mo_5Si_3 was detected in the area of the thin oxide layer, as shown in Fig. 13b [70]. The internal coating is very dense and uniform, and the bonding between layers is good, as shown in Fig. 13f. This indicates that the addition of B improves the fluidity of SiO_2, and promotes the formation of protective B_2O_3-SiO_2 film on the coating surface [71, 72]. The oxidized Ge-modified silicide coating has a smooth and compact surface, which is composed of dark gray glass phase (SiO_2) and light gray lamellar phase (TiO_2), as shown in Fig. 13c [60]. Its oxide layer is uniform and dense, with a thickness of about 50–60 μm, and trace GeO_2 particles are detected in it. The researches show that generation of GeO_2 can effectively reduce the viscosity of SiO_2 at high temperature and improve its fluidity, which is improving the self-healing ability of the coating under high temperature oxidation [73].

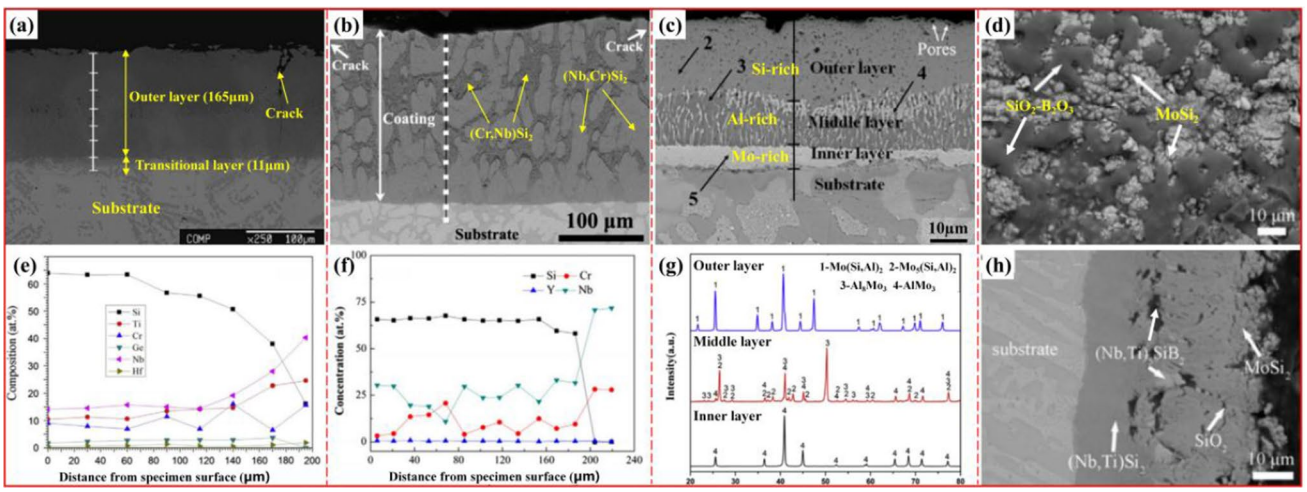

Fig. 12 Cross-section morphology and composition analysis of different coatings on Nb-based alloys; Ge-modified silicide **a** and **e** [60], Y-modified silicide **b** and **f** [64], cross-sectional morphology **c** and XRD test results **g** of the Mo-Si-Al coating [65], BSE pictures of surface **d** and cross-sectional **h** of the Mo-Si-B coating [66]

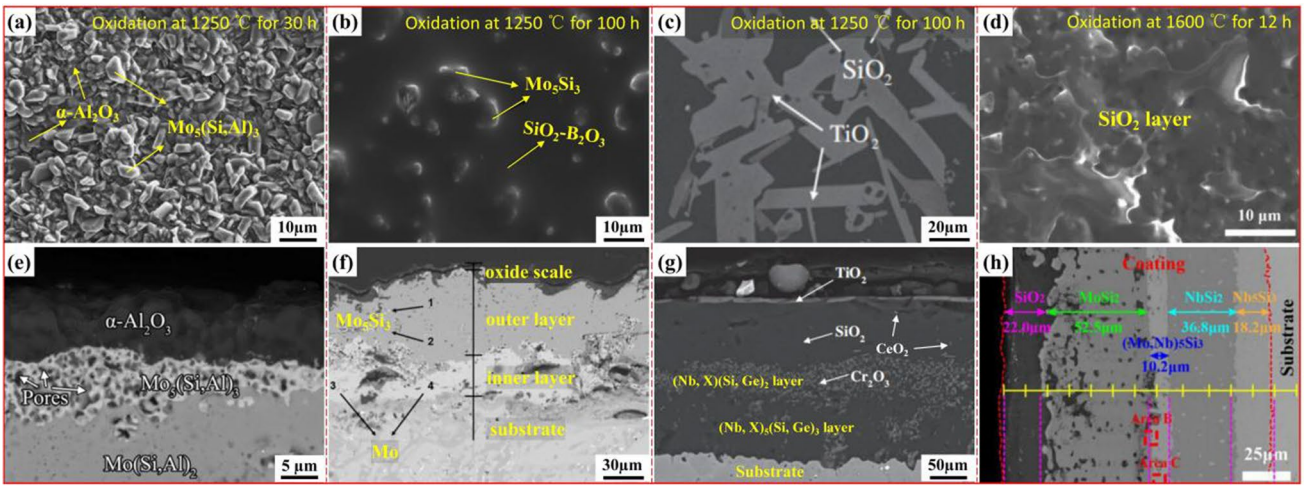

Fig. 13 The oxidized surface and corresponding cross-sections of the various silicide coatings modified by single element on Nb and Nb-based alloys under different conditions; Mo-Si-Al coating **a** and **e** [64], Mo-Si-B coating **b** and **f** [70], Ge-modified silicide coating **c** and **g** [60], Ce-modified $MoSi_2$-$NbSi_2$ coating **d** and **h** [74]

Xiao et al. [74] researched the affect of Ce element on the oxidation behavior of $MoSi_2$-$NbSi_2$ composite coating at high temperature. It is observed that the oxidized surface of the Ce-modified $MoSi_2$-$NbSi_2$ coating was covered with a layer of molten SiO_2 and granular bulges, the interior of the coating is very dense, and the layers are closely bonded, as shown in Fig. 13d and h, respectively. The surface of the oxidized $MoSi_2$-$NbSi_2$ coating has more granular bulges than that of the modified coating, and their Rsa are 2.027 μm and 1.776 μm, respectively, as shown in Fig. 14. This may be related to the finer surface grains of the modified coating. Further study showed that the average oxidation service life of the modified coating at 1600 °C was 28.5 h, slightly higher than 24.7 h of the $MoSi_2$-$NbSi_2$ coating. Furthermore, the exposure time is proportional to the square of the mass change per unit area (Δm/S) of the coating, and the coatings oxidation parabolic constant kp of the are calculated, as shown in Fig. 15 [75]. Which is due to that element Ce can refine the grain size of the coating, optimize the structure of the coating, and prolong the high-temperature oxidation service life of the coating [76].

3.2 Silicide Coating Modified by Composite Elements

3.2.1 Microstructure and Phase Composition of the Coatings

The images of silicide coating modified by composite element are shown in Fig. 16. It can be seen that the average grain size of Si–Ge–Y coating is only 0.84 μm, which is significantly lower than the 2.47 μm of Si-Ge coating, as shown in Fig. 16a and b. This is due to that the solubility of element Y in the grain is low, and the nanoscale $Y_3Al_5O_{12}$ particles are distributed at the grain boundary, which makes the Si–Ge–Y coating has a smaller grain size. The Si–Ge–Y coating is consists of a dense outer layer and a continuous transition layer, and their thickness are 179 μm and 12.1 μm,

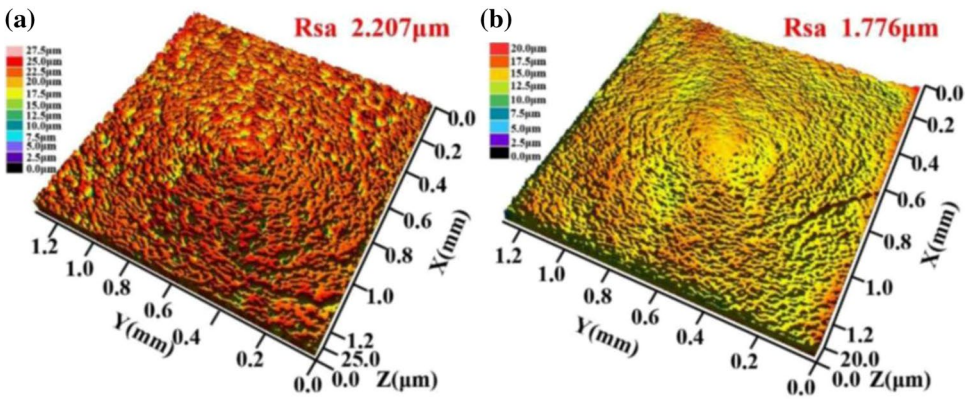

Fig. 14 Surface roughness analysis of different coatings after oxidation at 1600 °C for 12 h; $MoSi_2$-$NbSi_2$ coating **a**, Ce modified $MoSi_2$-$NbSi_2$ coating **b** [74]

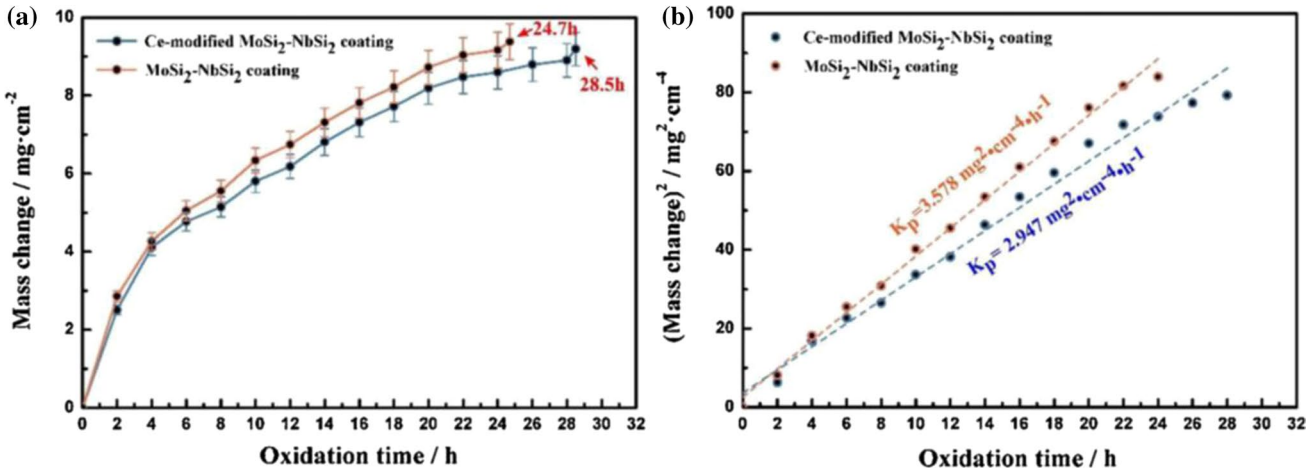

Fig. 15 Weight gains **a** and square of weight gains **b** of $MoSi_2$-$NbSi_2$ coatings with and without CeO_2 after oxidation at 1600 °C [74]

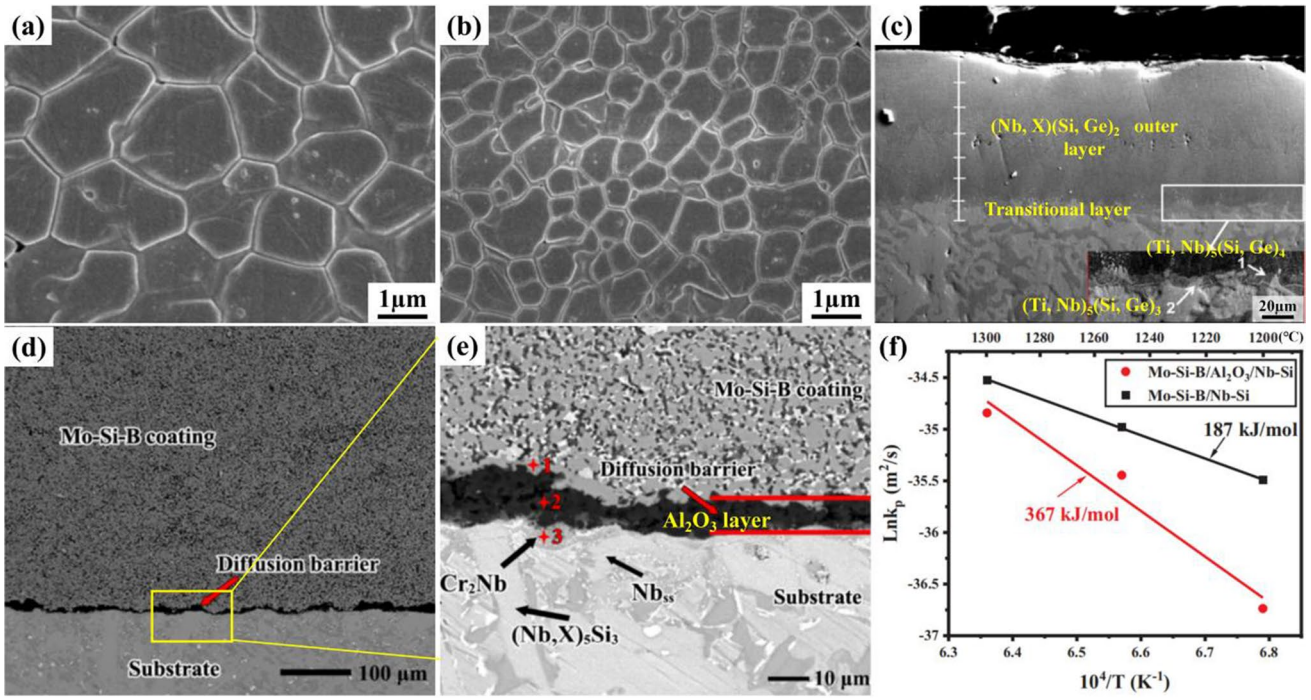

Fig. 16 Surface FESEM image of Si-Ge coating **a**, surface **b** and cross-sectional **c** FESEM images of Si–Ge–Y coating [77]. Cross-sectional images of Mo-Si-B/Al_2O_3 composite coating **d** and the magnified view of the its IDZ **e**. Plot of ln(kp) vs. 1/T for the IDZ in samples with and without Al_2O_3 diffusion barrier **f** [80]

respectively, as shown in Fig. 16c. The outer layer of the coating is made of $(Nb,X)(Si,Ge)_2$, while the transition layer is composed of dark gray $(Ti,Nb)_5(Si,Ge)_4$ phase and bright gray $(Nb,X)_5(Si,Ge)_3$ phase and the proportion of the two phases is 66% and 34%, respectively [77]. This indicates that the Si and Ge elements content are gradually reduces in the process of spreading to the substrate [78].

Plasma-physical vapor deposition (PS-PVD) combines the advantages of traditional plasma spraying and physical vapor deposition, which is a thermal barrier coatings(TBCs) preparation technology with broad application prospects. The principle of this process is to add spray powder to plasma gun, heat the material to liquid or vaporized state with low pressure plasma arc as heat source, and then transport it to the surface of the substrate through plasma air flow to form coating. The whole process is carried out in a vacuum chamber or in a protective atmosphere of inert gas, as shown in Fig. 17a [79]. Hou et al. [80] produced the

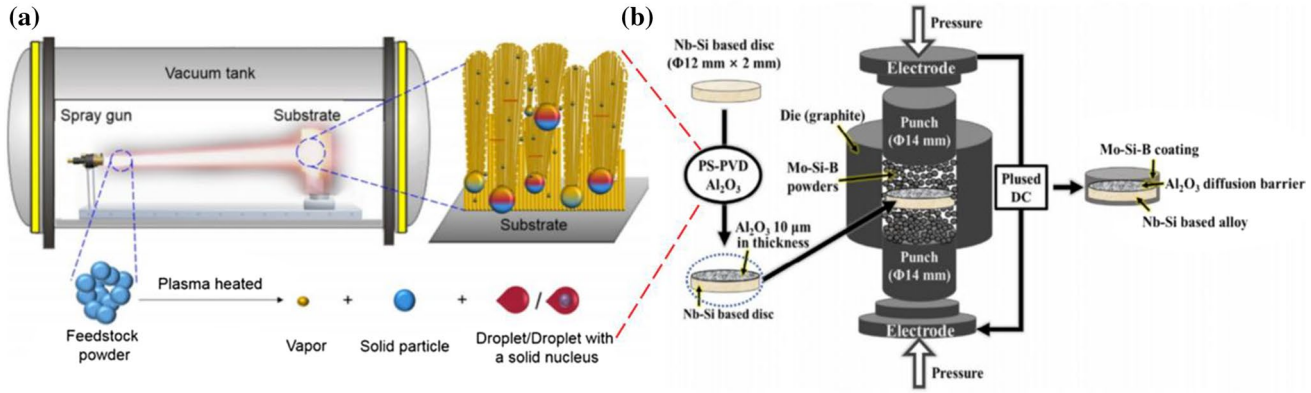

Fig. 17 Illustration of PS-PVD process **a** [79], schematic diagram of Mo-Si-B/Al_2O_3 coating preparation **b** [80]

Mo-Si-B/Al_2O_3 coating on Nb-Si based alloy by PS-PVD followed by spark plasma sintering (SPS) technology, successively. The preparation process of the coating is shown in Fig. 17b. Firstly, a Al_2O_3 coating with a thickness of 10 μm was deposited on the alloy surface by PS-PVD technique. Then the molybdenum, silicon and boron powders prepared in proportion are mixed evenly through ball milling. The deposited sample and mixed powder were put into SPS equipment (Model 1050) and sintered at 1300 °C for 5 min in Ar atmosphere, then the Mo-Si-B/Al_2O_3 coating will be obtained at a pressure of 40 MPa [80]. The Mo-Si-B/Al_2O_3 coating is composed of dense Mo-Si-B outer layer and continuous Al_2O_3 transition layer, as shown in Fig. 16d. The main components at point 1, 2 and 3 in the transition layer of the coating are $MoSi_2$, Al_2O_3 and Cr_2Nb in turn, no elements from the substrate are detected in the Mo-Si-B layer, as shown in Fig. 16e. The Ar rhenius plots of kp of Mo-Si-B/Nb-Si and Mo-Si-B/Al_2O_3/Nb-Si samples are shown in Fig. 16f. It shows that the activation energy Q of the sample containing Al_2O_3 diffusion barrier is 367 kJ/mol, which is much higher than that of the sample without Al_2O_3. This means that Al_2O_3, as a diffusion barrier, can effectively delay the mutual diffusion between the coating and substrate [81].

3.2.2 Oxidation Properties of the Coatings

The images of the oxidized silicified coatings modified by composite elements are shown in Fig. 18. It is observed that the surface of coatings are composed of two phases with significantly different brightness, namely dark gray flaky phase and bright light gray granular phase, as shown in Fig. 18a–c. Table 1 provides the EDS detection results at each point in a typical region of surface of the coatings, from which we can be inferred that their components are mainly SiO_2 and TiO_2 with a small amount of Al_2O_3 and Cr_2O_3. This indicates that Ti, Al, Cr and other elements diffuse outward faster in the oxidation process [78, 82, 83]. The oxidized coating is composed of an oxide outer layer, a $(Nb,X)(Si,Ge)_2$ middle layer and a $(Ti,Nb)_5Si_4$ transition layer. Compared to the oxidation before, the thickness of middle layer decreases obviously, and a mass of pores are discovered in the outer coating. This is related to the decomposition of silicides and Kirkendall effects caused by the spread of Si, Ti and Al [84]. The existence of these holes releases the thermal stress in the coating and effectively avoids the generation of cracks [85, 86]. What is noteworthy is that the thickness of $(Ti,Nb)_5Si_4$ layer increases significantly with the interdiffusion of the elements in each layer. The interior of all coatings is uniform and dense, demonstrating good metallurgical bonding with the substrate, as shown in Fig. 18d–f [77, 82, 83].

Further researcher shows that that the oxidation rate of Si–Ge–Y coating is slightly higher than that of Si-Ge coating in the initial oxidation stage, this is related to the smaller grain size of the coating. However, the oxidation rate of Si–Ge–Y coating is gradually lower than that of Si-Ge coating as the oxidation reaction enters the stable stage. The Δm/S of the two coatings oxidized for 100 h are 2.78 mg·cm^{-2} and 5.42 mg·cm^{-2}, respectively, as shown in Fig. 19a. It shows that the formation of $Y_3Al_5O_{12}$ particles at the grain boundary refines the grain size and promotes the formation of protective SiO_2 and GeO_2 oxide films on the surface of the coating, which makes the Si–Ge–Y coating has a better oxidation resistance than that of Si-Ge coating [77]. It is observed that the $(\Delta m/S)^2$ of the coatings are approximately linear with time, as shown in Fig. 19b. Which is indicating that the oxidation of the coating follows a parabolic law [87].

4 Oxidation and Failure Mechanisms of the Coatings

Figure 20 shows the oxidation and failure mechanisms of various coatings on Nb and its alloys. It can be seen that the coating consumption in the oxidation process not only comes

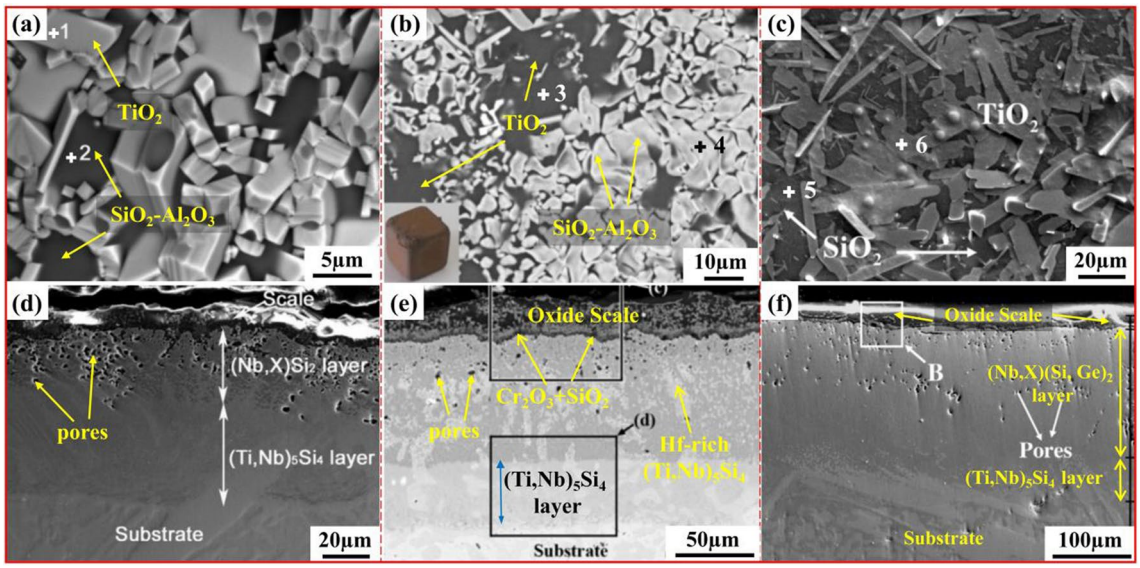

Fig. 18 The oxidized surface and corresponding cross-sections of the various composite element modified silicide coatings on niobium and its alloys at 1250 °C for 100 h; Si–Al–Y coating **a** and **d** [82], Si–B–Y coating **b** and **e** [83], Si–Ge–Y coating **c** and **f** [77]

Table 1 Chemical composition of the phases in Fig. 15a–c, determined by EDS analyses

Substrate	Coating types	Position	The types and content of elements (at%)								Refs.
			O	Si	Ti	Nb	Cr	Al	Hf	Y	
Nb-16Si-22Ti-17Cr-2Al-2Hf	Si–Al–Y	1	73.22	0.18	24.47	0.72	0.65	0.51	0.24	–	82
		2	68.80	19.22	4.13	–	0.47	6.74	0.11	0.52	
Nb-20Ti-16Si-6Cr-5Hf-4Al	Si–B–Y	3	65.8	1.8	15.9	9.6	3.5	2.0	1.2	0.2	83
		4	66.8	20.6	2.8	2.4	1.2	5.8	0.3	0.1	
Nb-16Si-22Ti-17Cr-2Al-2Hf	Si–Ge–Y	5	67.3	29.5	1.7	–	1.6	–	–	–	78
		6	72.4	3.3	22.4	–	2.0	–	–	–	

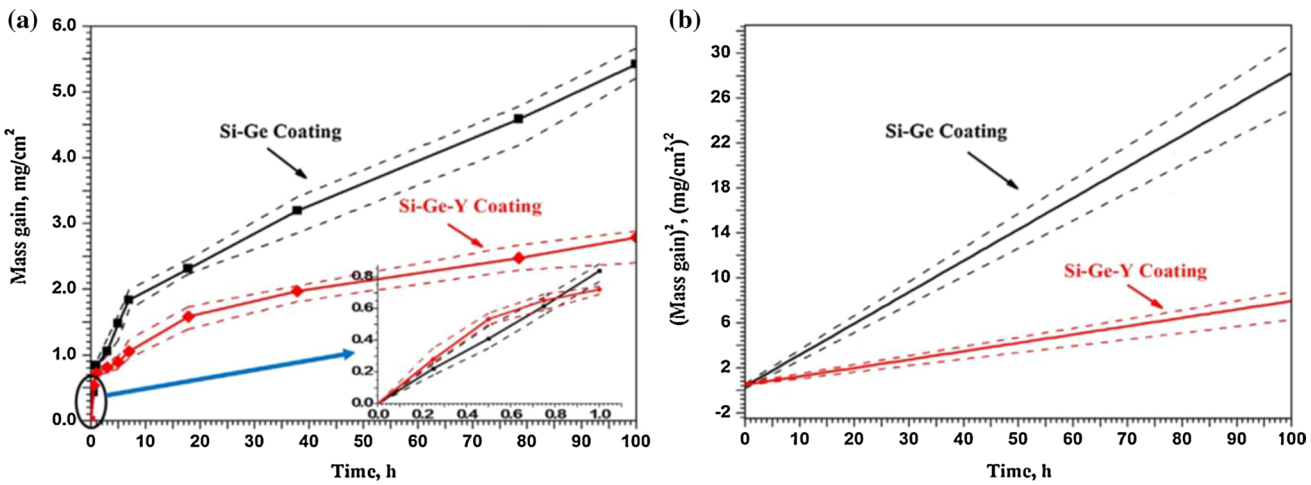

Fig. 19 Weight gains **a** and square of weight gains **b** of the coatings exposure at 1250 °C for 100 h [77]

from the surface oxidation reaction, but also depends on the diffusion growth of the inner interface layer. For the single coating, with the formation and volatilization of NbO_2/(MoO_3) during oxidation process, its porosity and the surface roughness increases rapidly, which is not conducive to the formation of protective oxide film on its surface. In addition, due to the single composition and structure of coating, a mass of cracks will appear inside its internal during the oxidation process, which is greatly deteriorates the high temperature oxidation resistance of the coating, as shown in Fig. 20a and b. For the composite silicide coating, the $ReSi_2$ layer can act as a barrier to inhibit the diffusion of Si element and maintain the structural integrity of the coating. Mullite fills the pores on the surface of the coating and promotes the formation of a continuous and stable oxide film. The W element can combine with elements such as Mo, Si and Nb to form (Mo, W)Si_2, (Mo, W)$_5Si_3$ and (Mo, W, Nb)$_5Si_3$ compounds inside the coating, which can uniform the coating composition and inhibit the diffusion of Si element. Moreover, the solid solution phases of (Mo, W)Si_2 formed on the coating surface have similar CTE values to that of SiO_2, which can alleviate the surface cracking of the coating to a certain extent, as shown in Fig. 20c and d.

The addition of modified elements makes the coating have more uniform composition, compact structure and more stable oxidation resistance. The Al element is preferred to be oxidized to form protective a-Al_2O_3 oxide film, which reduces the oxygen partial pressure on the surface of the coating and slows down the oxidation rate of the coating. Furthermore, the Al_2O_3 as the interface layer between the coating and the substrate can effectively alleviate the mutual diffusion between them and maintain the integrity of the coating structure. The B and Ge elements can reduce the viscosity of SiO_2 at a high temperature, enhance its fluidity, and promote the formation of a smooth and dense oxide layer on the surface of the coatings. The Ce element can refine the grain size of the coating, optimize the structure of the coating, and enhance the self-healing ability of the coating under high temperature oxidation. The $Y_3Al_5O_{12}$ particles formed by the combination of Y element and Al in the oxidation process can effectively refine the grain size of the coating, reduce its surface roughness and promote the formation of a smooth oxide film on its surface. In addition, Some pores generated in the coating during the oxidation process effectively release the thermal stress and avoid the generation of cracks, as shown in Fig. 20 e and f.

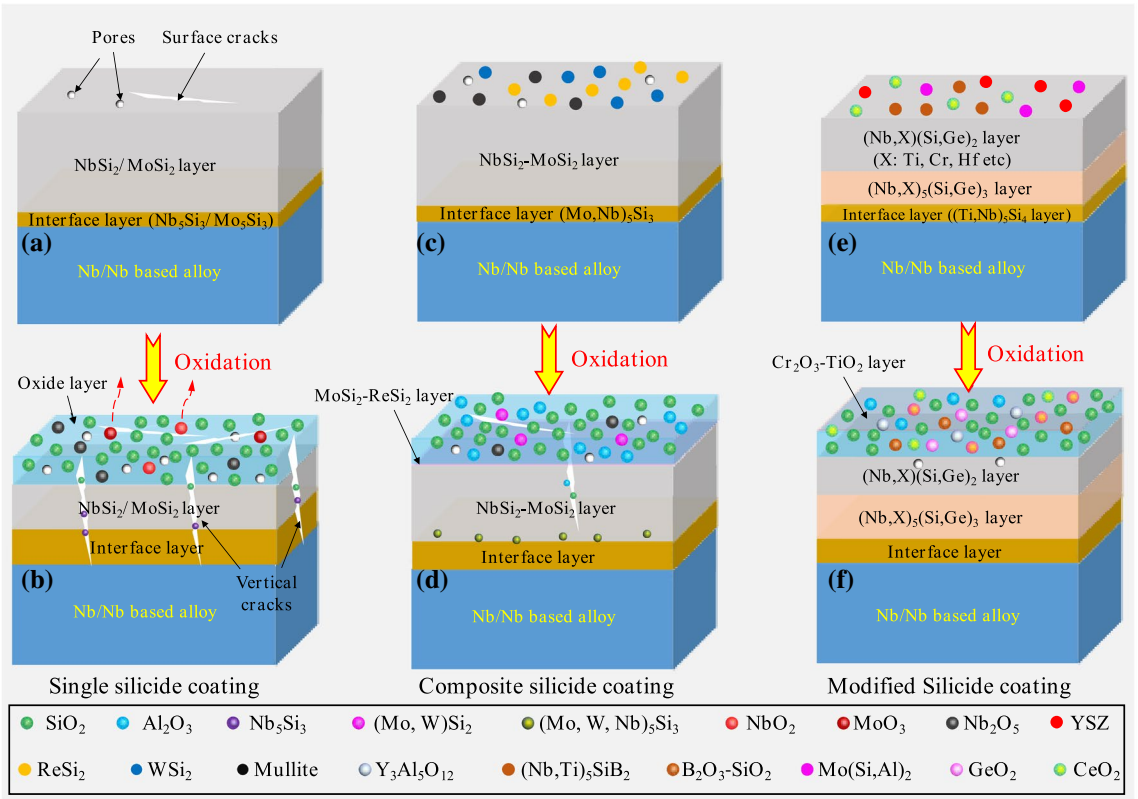

Fig. 20 Schematic diagram of oxidation mechanism of silicide coating on Nb and Nb-based alloys

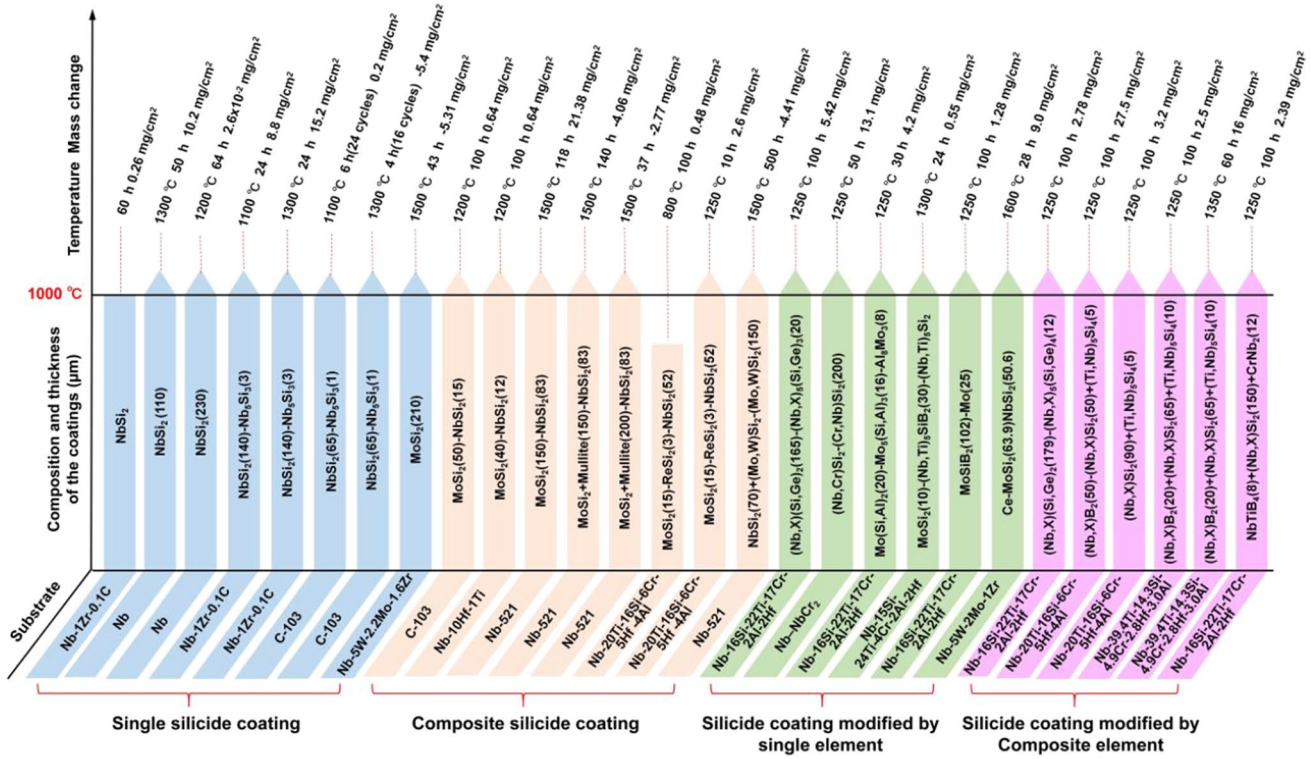

Fig. 21 Overview of the composition and oxidation characteristics of surface coatings on Nb and Nb-based alloys

5 Conclusions and Prospect

In this paper, the application of various anti-oxidation coatings on Nb and its alloy are introduced in detail, the composition and oxidation characteristics of coatings are summarized as shown in Fig. 21. There is no doubt that the composition and structure of the coatings have an important effect on their oxidation behavior. Due to the single composition and structure of coating, various defects generated during the oxidation process make the single silicide coating unable to be used at high temperatures (1500 °C and above) for long periods of time. Compared with single coating, the structure of composite coating is further optimized. However, defects such as cracks in the coating can not be avoided in the oxidation process as usual. At the same time, the rapid growth of the interface layer also accelerates the consumption of the coating. All these problems result in a significant reduction in the oxidation life of such coatings. The modified silicide coatings prepared by two-step process have smooth surface, compact structure and uniform composition. This makes their have excellent self-healing ability and stable oxidation resistance at high temperature.

By optimizing the coating preparation process, combining two or more processes organically to eliminate the problems existing in the application process of a single process. This will make the coatings have a more uniform composition, denser structure and lower surface roughness. In addition, the coating structure can be further optimized by adding appropriate amount of modified elements or introducing the second phases. It can not only delay the diffusion of Si elements to the substrate, inhibit the formation of low silicon compounds (Nb_5Si_3, Mo_5Si_3) with poor oxidation resistance, but also promote the formation of continuous and dense anti-oxidation film on the surface of coating, and reduce the generation of volatile oxides (NbO_2, MoO_3 etc.). Therefore, the modified silicide coatings obtained by multi-step have a bright application prospect, which will be an important development direction in this field in the future.

Author contributions The manuscript was written through contributions of all authors. YYZ: Conceptualization, Investigation, and Supervision. YYZ and TF: Writing original draft and image processing. TF, KKC, and JW: Validation, Resources, Investigation, Writing—review and editing. XZ, KCZ, LHY and FQS: Visualization, Writing—review and editing. All authors have given approval to the final version of the manuscript.

Funding This work was supported by the Anhui Province Science Foundation for Excellent Young Scholars (2108085Y19) and the National Natural Science Foundation of China (No. 51604049).

Data Availability The data that support the findings of this study are available from the corresponding author upon reasonable request.

References

1. F. Shen, Y. Zhang, L. Yu, T. Fu, J. Wang, H. Wang, K. Cui, Microstructure and oxidation behavior of Nb-Si-based alloys for ultrahigh temperature applications: a comprehensive review. Coatings **11**(11), 1373 (2021). https://doi.org/10.3390/coatings11111373
2. X. Zhang, T. Fu, K.K. Cui, Y.Y. Zhang, F.Q. Shen, J. Wang, L.H. Yu, H.B. Mao, A. Tolstoguzov, The protection, challenge, and prospect of anti-oxidation coating on the surface of niobium alloy. Coatings **11**(7), 742 (2021). https://doi.org/10.3390/coatings11070742
3. J. Wang, Y. Zhang, L. Yu, K. Cui, T. Fu, H. Mao, Effective separation and recovery of valuable metals from waste Ni-based batteries: A comprehensive review. Chem. Eng. J. **439**, 135767 (2022). https://doi.org/10.1016/j.cej.2022.135767
4. J.H. He, X.P. Guo, Y.Q. Qiao, Effect of Zr content on the structure and oxidation resistance of silicide coatings prepared by pack cementation technique. Corros. Sci. **147**, 152–162 (2019). https://doi.org/10.3390/coatings12020141
5. D.Z. Yao, C.G. Zhou, J.Y. Yang, H.F. Chen, Experimental studies and modeling of the oxidation of multiphase niobium-base alloys. Corros. Sci. **51**(11), 2617–2619 (2009). https://doi.org/10.1016/j.corsci.2009.06.053
6. Y.X. Li, J.H. Nie, Y.X. Yang, P.K. Bai, H.J. Zhang, Z.Y. Zhao, S.Z. Wei, J. Cai, Q.F. Guan, High-temperature oxidation behavior of nicocraly coatings deposited by laser cladding on 304 stainless steel. Met. Mater. Int. **28**, 412–420 (2022). https://doi.org/10.1007/s12540-020-00927-y
7. L. Yu, F. Shen, T. Fu, Y. Zhang, K. Cui, J. Wang, X. Zhang, Microstructure and oxidation behavior of metal-modified Mo-Si-B alloys a review. Coatings **11**(10), 1256 (2021). https://doi.org/10.3390/coatings11101256
8. L. Yu, Y. Zhang, T. Fu, J. Wang, K. Cui, F. Shen, Rare earth elements enhanced the oxidation resistance of Mo-Si-based alloys for high temperature application: a review. Coatings **11**(9), 1144 (2021). https://doi.org/10.3390/coatings11091144
9. S. Zhang, X.P. Guo, Alloying effects on the microstructure and properties of Nb-Si based ultrahigh temperature alloys. Intermetallics **70**, 33–44 (2016). https://doi.org/10.1016/j.intermet.2015.12.002
10. G. Kim, H. Shin, J. Lee, W. Lee, A review on silicide-based materials: thermoelectric and mechanical properties. Met. Mater. Int. **27**, 2205–2219 (2021). https://doi.org/10.1007/s12540-020-00609-9
11. Y.C. Yan, H.S. Ding, Y.W. Kang, J.X. Song, Microstructure evolution and mechanical properties of Nb-Si based alloy processed by electromagnetic cold crucible directional solidification. Mater. Des. **55**, 450–455 (2014). https://doi.org/10.1016/j.matdes.2013.10.017
12. Z.P. Sun, J.M. Guo, C. Zhang, X.P. Guo, X.D. Tian, Effect of Ti and Al interaction on microstructures and mechanical properties of the Nb-Ti-Si-Al alloys. Rare Metal Mater. Eng. **45**(7), 1678–1682 (2016). https://doi.org/10.1016/S1875-5372(16)30139-4
13. I. Grammenos, P. Tsakiropoulos, Study of the role of Hf, Mo and W additions in the microstructure of Nb–20Si silicide based alloys. Intermetallics **19**(10), 1612–1621 (2011). https://doi.org/10.1016/j.intermet.2011.06.008
14. S.S. Zhang, Y.C. Liu, T.W. Xu, M.X. Sun, Q. Zhang, Y. Wan, Effect of texture and microstructure on tensile behaviors in the polycrystalline pure niobium. Met. Mater. Int. **27**, 4023–4034 (2021). https://doi.org/10.1007/s12540-020-00925-0
15. D.L. Pu, Y. Pan, Influence of high pressure on the structure, hardness and brittle-to-ductile transition of $NbSi_2$ ceramics. Ceram. Int. **47**(2), 2311–2318 (2021). https://doi.org/10.1016/j.ceramint.2020.09.073
16. G.M. Karthik, H.S. Kim, Heterogeneous aspects of additive manufactured metallic parts: a review. Met. Mater. Int. **27**, 1–39 (2021). https://doi.org/10.1007/s12540-020-00931-2
17. Y. Pan, Structural Prediction and overall performances of $CrSi_2$ disilicides: DFT investigations. ACS Sustain. Chem. Eng. **8**, 11024–11030 (2020). https://doi.org/10.1021/acssuschemeng.0c04737
18. X. Fang, X.P. Guo, Y.Q. Qiao, Effect of Ti addition on microstructure and crystalline orientations of directionally solidified Nb–Si based alloys. Intermetallics **122**, 106798 (2020). https://doi.org/10.1016/j.intermet.2020.106798
19. I. Grammenos, P. Tsakiropoulos, Study of the role of Al, Cr and Ti additions in the microstructure of Nb-18Si-5Hf base alloys. Intermetallics **18**(2), 242–253 (2010). https://doi.org/10.1016/j.intermet.2009.07.020
20. Y.Y. Zhang, J.M. Qie, K.K. Cui, T. Fu, X.L. Fan, J. Wang, X. Zhang, Effect of hot dip silicon-plating temperature on microstructure characteristics of silicide coating on tungsten substrate. Ceram. Int. **46**(4), 5223–5228 (2020). https://doi.org/10.1016/j.ceramint.2019.10.270
21. S. Zhang, X.P. Guo, Effects of Cr and Hf additions on the microstructure and properties of Nb silicide based ultrahigh temperature alloys. Mater. Sci. Eng. A **638**, 121–131 (2015). https://doi.org/10.1016/j.msea.2015.04.003
22. Y.Y. Zhang, T. Fu, L.H. Yu, F.Q. Shen, J. Wang, K.K. Cui, Improving oxidation resistance of TZM alloy by deposited Si–MoSi2 composite coating with high silicon concentration, Ceram. Int. (2022). https://doi.org/10.1016/j.ceramint.2022.04.080
23. Y.Y. Zhang, S. Hussain, K.K. Cui, T. Fu, J. Wang, M.S. Javed, Y. Lv, B. Aslam, Microstructure and mechanical properties of $MoSi_2$ coating deposited on Mo substrate by hot dipping processes. J. Nanoelectron. Optoelectron. **14**(12), 1680–1685 (2019). https://doi.org/10.1166/jno.2019.2676
24. Y.Y. Zhang, Y.G. Li, C.G. Bai, Microstructure and oxidation behavior of Si-$MoSi_2$ functionally graded coating on Mo substrate. Ceram. Int. **43**(8), 6250–6256 (2017). https://doi.org/10.1016/j.ceramint.2017.02.024
25. F. Shen, L. Yu, T. Fu, Y. Zhang, H. Wang, K. Cui, J. Wang, S. Hussain, N. Akhtar, Effect of the Al, Cr and B elements on the mechanical properties and oxidation resistance of Nb-Si based alloys: a review. Appl. Phys. A **127**, 852 (2021). https://doi.org/10.1007/s00339-021-05013-7
26. Y.Y. Zhang, T. Fu, K.K. Cui, F.Q. Shen, J. Wang, L.H. Yu, H.B. Mao, Evolution of surface morphology, roughness and texture of tungsten disilicide coatings on tungsten substrate. Vacuum **14**, 110297 (2021). https://doi.org/10.1016/j.vacuum.2021.110297
27. K. Cui, H. Mao, Y. Zhang, J. Wang, H. Wang, T. Tan, T. Fu, Microstructure, mechanical properties, and reinforcement mechanism of carbide toughened ZrC-based ultra-high temperature ceramics. Compos. Interfaces (2022). https://doi.org/10.1080/09276440.2021.2012409
28. Y.Y. Zhang, K.K. Cui, Q.J. Gao, S. Hussain, Y. Lv, Investigation of morphology and texture properties of WSi_2 coatings on W substrate based on contact-mode AFM and EBSD. Surf. Coat. Technol. **396**(25), 125966 (2020). https://doi.org/10.1016/j.surfcoat.2020.125966
29. K. Zelenitsas, P. Tsakiropoulos, Effect of Al, Cr and Ta additions on the oxidation behaviour of Nb-Ti-Si in situ composites at 800 °C. Mater. Sci. Eng. A **416**, 269–280 (2006). https://doi.org/10.1016/j.msea.2005.10.017
30. T. Fu, F.Q. Shen, Y.Y. Zhang, L.H. Yu, K.K. Cui, J. Wang, X. Zhang, Oxidation protection of high-temperature coatings on the

surface of Mo-Based alloys-a review. Coatings **12**(2), 141 (2022). https://doi.org/10.3390/coatings12020141
31. Y.Y. Zhang, L.H. Yu, T. Fu, J. Wang, F.Q. Shen, K.K. Cui, Microstructure evolution and growth mechanism of Si-MoSi2 composite coatings on TZM (Mo-0.5Ti-0.1Zr-0.02 C) alloy. J. Alloys Compd. **894**(15), 162403 (2022). https://doi.org/10.1016/j.jallcom.2021.162403
32. Y.Y. Zhang, W.J. Ni, Y.G. Li, Effect of siliconizing temperature on microstructure and phase constitution of Mo–$MoSi_2$ functionally graded materials. Ceram. Int. **44**(10), 11166–11171 (2018). https://doi.org/10.1016/j.ceramint.2018.03.136
33. X. Tian, X. Guo, Z. Sun, Z. Yin, L. Wang, Formation of B-modified $MoSi_2$ coating on pure Mo prepared through HAPC process. Int. J. Refract. Metals Hard Mater. **45**, 8–14 (2014). https://doi.org/10.1016/j.ijrmhm.2014.03.003
34. B. Vishwanadh, R.H. Naina, S. Majumdar, R. Tewari, G.K.A. Dey, A study on the oxidation behavior of Nb alloy (Nb-1 pct Zr-0.1 pct C) and silicide-coated Nb alloys. Metall. Mater. Trans. A **44**, 2258–2269 (2013). https://doi.org/10.1007/s11661-012-1554-1
35. L. Liu, H. Lei, J. Gong, C. Sun, Deposition and oxidation behaviour of molybdenum disilicide coating on Nb based alloys substrate by combined AIP/HAPC processes. Ceram. Int. **45**(8), 10525–10529 (2019). https://doi.org/10.1016/j.ceramint.2019.02.115
36. J.C. Cheng, S. Yi, J.S. Park, Oxidation behavior of Nb-Si-B alloys with the $NbSi_2$ coating layer formed by a pack cementation technique. Int. J. Refract Metal Hard Mater. **41**, 103–109 (2013). https://doi.org/10.1016/j.ijrmhm.2013.02.010
37. S. Majumdar, J. Kishor, B. Paul, R.C. Hubli, J.K. Chakravartty, Isothermal oxidation behavior and growth kinetics of silicide coatings formed on Nb-1Zr-0.1C alloy. Corros. Sci. **95**, 100–109 (2015). https://doi.org/10.1016/j.corsci.2015.02.035
38. E.H. Jordan, L. Xie, M. Gell, N.P. Padture, B. Cetegen, A. Ozturk, X. Ma, J. Roth, T.D. Xiao, P.E.C. Bryant, Superior thermal barrier coatings using solution precursor plasma spray. J. Therm. Spray Technol. **13**, 57–65 (2004). https://doi.org/10.1007/s11666-004-0050-6
39. L. Sun, Q.G. Fu, X.Q. Fang, J. Sun, A $MoSi_2$-based composite coating by supersonic atmospheric plasma spraying to protect Nb alloy against oxidation at 1500 °C. Surf. Coat. Technol. **325**, 182–190 (2018). https://doi.org/10.1016/j.surfcoat.2018.07.091
40. D.L. Pu, Y. Pan, First-principles investigation of oxidation mechanism of Al-doped Mo_5Si_3 silicide. Ceram. Int. **48**(8), 11518–11526 (2022). https://doi.org/10.1016/j.ceramint.2022.01.007
41. J. Yan, L. Liu, Z. Mao, H. Xu, Y. Wang, Effect of spraying powders size on the microstructure, bonding strength, and microhardness of $MoSi_2$ coating prepared by air plasma spraying. J. Therm. Spray Technol. **23**, 934–939 (2014). https://doi.org/10.1007/s11666-014-0120-3
42. Y.J. Choi, J.K. Yoon, G.H. Kim, W.Y. Yoon, J.M. Doh, K.T. Hong, High temperature isothermal oxidation behavior of $NbSi_2$ coating at 1000–1450 °C. Corros. Sci. **129**, 102–114 (2017). https://doi.org/10.1016/j.corsci.2017.10.002
43. J. Sun, T. Li, G.P. Zhang, Q.G. Fu, Different oxidation protection mechanisms of HAPC silicide coating on niobium alloy over a large temperature range. J. Alloy. Compd. **790**, 1014–1022 (2019). https://doi.org/10.1016/j.jallcom.2019.03.229
44. Y.Y. Zhang, K.K. Cui, T. Fu, J. Wang, F.Q. Shen, X. Zhang, L.H. Yu, Formation of MoSi2 and Si/MoSi2 coatings on TZM (Mo-0.5Ti-0.1Zr-0.02C) alloy by hot dip silicon-plating method. Ceram. Int. **47**(16), 23053–23065 (2021). https://doi.org/10.1016/j.ceramint.2021.05.020
45. L. Liu, H.Q. Zhang, H. Lei, H.Q. Li, J. Gong, C. Sun, Influence of different coating structures on the oxidation resistance of $MoSi_2$ coatings. Ceram. Int. **46**(5), 5993–5997 (2020). https://doi.org/10.1016/j.ceramint.2019.11.055
46. L. Sun, Q.G. Fu, J. Sun, G.P. Zhang, Comparison investigation of hot corrosion exposed to Na_2SO_4 salt and oxidation of $MoSi_2$-based coating on Nb alloy at 1000 °C. Surf. Coat. Technol. **385**, 125388 (2020). https://doi.org/10.1016/j.surfcoat.2020.125388
47. Y.L. Guo, L.N. Jia, B. Kong, F.X. Zhang, J.H. Liu, H. Zhang, Improvement in the oxidation resistance of Nb-Si based alloy by selective laser melting. Corros. Sci. **127**, 260–269 (2017). https://doi.org/10.1016/j.corsci.2017.08.022
48. S. Majumdar, J. Kishor, B. Paul, R.C. Hubli, J.K. Chakravartty, Isothermal oxidation behavior and growth kinetics of silicide coatings formed on Nb-1Zr-0.1C alloy. Corros. Sci. **95**, 100–109 (2015). https://doi.org/10.1016/j.corsci.2015.02.035
49. Y. Pan, W.M. Guan, The hydrogenation mechanism of PtAl and IrAl thermal barrier coatings from first-principles investigations. Int. J. Hydrog. Energy **45**(38), 20032–20041 (2020). https://doi.org/10.1016/j.ijhydene.2020.04.290
50. G. Yue, X.P. Guo, Y.Q. Qiao, Microstructure and oxidation behaviors at 800°C and 1250°C of $MoSi_2$/$ReSi_2$/$NbSi_2$ compound coating prepared by electrodeposition and then pack cementation. Ceram. Int. **45**(9), 11739–11748 (2019). https://doi.org/10.1016/j.ceramint.2019.03.050
51. A. Allam, P. Boulet, M.C. Record, Linear thermal expansion coefficients of higher manganese silicide compounds. Phys. Proc. **55**, 24–29 (2014). https://doi.org/10.1016/j.phpro.2014.07.004
52. G.P. Zhang, J. Sun, Q.G. Fu, Effect of mullite on the microstructure and oxidation behavior of thermal sprayed $MoSi_2$ coating at 1500 °C. Ceram. Int. **46**(8), 10058–10066 (2020). https://doi.org/10.1016/j.ceramint.2019.12.273
53. G.P. Zhang, J. Sun, Q.G. Fu, Microstructure and oxidation behavior of plasma sprayed WSi_2-mullite $MoSi_2$ coating on niobium alloy at 1500 °C. Surf. Coat. Technol. **400**, 126210 (2020). https://doi.org/10.1016/j.surfcoat.2020.126210
54. M.Z. Alam, A.S. Rao, D.K. Das, Microstructure and high temperature oxidation performance of silicide coating on Nb-based alloy C-103. Oxid. Met. **73**, 513–530 (2010). https://doi.org/10.1007/s11085-010-9190-x
55. G. Yue, X.P. Guo, Y.Q. Qiao, C.G. Zhou, Electrodeposition of Mo/Re duplex layer and preparation of $MoSi_2$/$ReSi_2$/$NbSi_2$ compound coating on Nb-Ti-Si based alloy. Corros. Sci. **153**, 283–291 (2019). https://doi.org/10.1016/j.corsci.2019.03.053
56. Y.Y. Zhang, J. Zhao, J.H. Li, J. Lei, X.K. Cheng, Effect of hot-dip siliconizing time on phase composition and microstructure of Mo-$MoSi_2$ high temperature structural materials. Ceram. Int. **45**(5), 5588–5593 (2019). https://doi.org/10.1016/j.ceramint.2018.12.018
57. M.T. Wang, Q.S. Zheng, A.Y. Chen, Y. Li, X.W. Zhang, D.L. Zhang, S. Jin, D.H. Xiong, W. Deng, Crystallization, thermal expansion and hardness of Y_2O_3–Al_2O_3–SiO_2 glasses. Ceram. Int. **47**(17), 25059–25066 (2021). https://doi.org/10.1016/j.ceramint.2021.05.236
58. A. Anagnostopoulos, A. Alexiadis, Y.L. Ding, Simplified force field for molecular dynamics simulations of amorphous SiO_2 for solar applications. Int. J. Therm. Sci. **160**, 106647 (2021). https://doi.org/10.1016/j.ijthermalsci.2020.106647
59. Y.Y. Zhang, K.K. Cui, T. Fu, J. Wang, J.M. Qie, X. Zhang, Synthesis WSi_2 coating on W substrate by HDS method with various deposition times. Appl. Surf. Sci. **511**, 145551 (2020). https://doi.org/10.1016/j.apsusc.2020.145551
60. W. Wang, B.F. Yuan, C.G. Zhou, Formation and oxidation resistance of germanium modified silicide coating on Nb based in situ composites. Corros. Sci. **80**, 164–168 (2014). https://doi.org/10.1016/j.corsci.2013.11.029
61. B. Voglewede, V.R. Rangel, S.K. Varma, The effects of uncommon silicides on the oxidation behavior of alloys from the

Nb–Cr–Si system. Corros. Sci. **61**, 123–133 (2012). https://doi.org/10.1016/j.corsci.2012.04.029
62. T. Fu, K.K. Cui, Y.Y. Zhang, J. Wang, X. Zhang, F.Q. Shen, L.H. Yu, H.B. Mao, Microstructure and oxidation behavior of anti-oxidation coatings on Mo-Based alloys through HAPC Process: a review. Coatings **11**(8), 883 (2021). https://doi.org/10.3390/coatings11080883
63. M. Fukumoto, Y. Matsumura, S. Hayashi, T. Narita, K. Sakamoto, A. Kasama, R. Tanaka, Coatings of Nb-based alloy by Cr and/or Al pack cementations and its oxidation behavior in Air at 1273–1473 K. Mater. Trans. **44**(4), 731–735 (2003). https://doi.org/10.2320/matertrans.44.731
64. Y.Q. Qiao, M.Y. Li, X.P. Guo, Development of silicide coatings over Nb–$NbCr_2$ alloy and their oxidation behavior at 1250 °C. Surf. Coat. Technol. **285**, 921–930 (2014). https://doi.org/10.1016/j.surfcoat.2014.07.058
65. Y. Liu, W. Shao, C.L. Wang, C.G. Zhou, Microstructure and oxidation behavior of Mo-Si-Al coating on Nb-based alloy. J. Alloy. Compd. **735**, 2247–2255 (2018). https://doi.org/10.1016/j.jallcom.2017.11.339
66. L.F. Su, O.L. Steffes, H. Zhang, J.H. Perepezko, An ultra-high temperature Mo-Si-B based coating for oxidation protection of Nb_{SS}/Nb_5Si_3 composites. Appl. Surf. Sci. **337**, 38–44 (2015). https://doi.org/10.1016/j.apsusc.2015.02.061
67. R. Sakidja, J.S. Park, J. Hamann, J.H. Perepezko, Synthesis of oxidation resistant silicide coating on Mo-Si-B alloys. Scripta Mater. **53**(6), 723–728 (2005). https://doi.org/10.1016/j.scriptamat.2005.05.015
68. T. Tabaru, K. Shobu, H. Hirai, S. Hanada, Influences of Al content and secondary phase of $Mo_5(Si, Al_)3$ on the oxidation resistance of Al-rich Mo(Si, A_l)2-base composites. Intermetallics **11**(7), 721–733 (2003). https://doi.org/10.1016/S0966-9795(03)00072-4
69. M.Z. Alam, B. Venkataraman, B. Sarma, D.K. Das, $MoSi_2$ coating on Mo substrate for short-term oxidation protection in air. J. Alloy. Compd. **487**(1), 335–340 (2009). https://doi.org/10.1016/j.jallcom.2009.07.141
70. J.Y. Wu, W. Wang, C.G. Zhou, Microstructure and oxidation resistance of Mo–Si–B coating on Nb based in situ composites. Corros. Sci. **87**, 421–426 (2014). https://doi.org/10.1016/j.corsci.2014.07.006
71. P. Ritt, R. Sakidja, J.H. Perepezko, Mo–Si–B based coating for oxidation protection of SiC-C composites. Surf. Coat. Technol. **206**(19–20), 4166–4172 (2012). https://doi.org/10.1016/j.surfcoat.2012.04.016
72. T. Feng, H.J. Li, X.H. Shi, X. Yang, Y.X. Li, X.Y. Yao, Sealing role of B_2O_3 in $MoSi_2$–$CrSi_2$–Si/B-modified SiC coating for C/C composites. Corros. Sci. **60**, 4–9 (2012). https://doi.org/10.1016/j.corsci.2012.04.018
73. C. Wang, W. Shao, W. Wang, C. Zhou, Oxidation behaviour of a Ge-modified silicide coating on an Nb-Si based alloy in the moderate temperature range. Corros. Sci. **163**, 108249 (2020). https://doi.org/10.1016/j.corsci.2019.108249
74. L.R. Xiao, X.J. Zhou, Y.F. Wang, R. Pu, G. Zhao, Z.Q. Shen, Y.L. Huang, S.N. Liu, Z.Y. Cai, X.J. Zhao, Formation and oxidation behavior of Ce-modified $MoSi_2$-$NbSi_2$ coating on niobium alloy. Corros. Sci. **173**, 108751 (2020). https://doi.org/10.1016/j.corsci.2020.108751
75. Z. Cai, D. Zhang, X. Chen, Y. Huang, Y. Peng, C. Xu, S. Huang, R. Pu, S. Liu, X. Zhao, L. Xiao, A novel ultra-high-temperature oxidation protective $MoSi_2$-$TaSi_2$ ceramic coating for tantalum substrate. J. Eur. Ceram. Soc. **39**(7), 2277–2286 (2019). https://doi.org/10.1016/j.jeurceramsoc.2019.02.037
76. V. Sreedhar, J. Das, R. Mitra, S.K. Roy, Influence of superficial CeO_2 coating on high temperature oxidation behavior of Ti–6Al–4V. J. Alloy. Compd. **519**, 106–111 (2012). https://doi.org/10.1016/j.jallcom.2011.12.118
77. W. Wang, C.G. Zhou, Characterization of microstructure and oxidation resistance of Y and Ge modified silicide coating on Nb-Si based alloy. Corros. Sci. **110**, 114–122 (2016). https://doi.org/10.1016/j.corsci.2016.04.026
78. S. Majumdar, P. Sengupta, G.B. Kale, I.G. Sharma, Development of multilayer oxidation resistant coatings on niobium and tantalum. Surf. Coat. Technol. **200**(12–13), 3713–3718 (2006). https://doi.org/10.1016/j.surfcoat.2005.01.034
79. B. Zhang, W. Song, L. Wei, Y. Xiu, H. Xu, D.B. Dingwell, H. Guo, Novel thermal barrier coatings repel and resist molten silicate deposits. Scripta Mater. **163**, 71–76 (2019). https://doi.org/10.1016/j.scriptamat.2018.12.028
80. Q.Y. Hou, W. Shao, M.F. Li, C.G. Zhou, Interdiffusion behavior of Mo-Si-B/Al_2O_3 composite coating on Nb-Si based alloy. Surf. Coat. Technol. **401**, 126243 (2020). https://doi.org/10.1016/j.surfcoat.2020.126243
81. C.L. Yeh, Y.H. Wang, Formation of zirconium silicide–Al_2O_3 composites from PTFE-assisted ZrO_2/Si/Al combustion synthesis. Vacuum **184**, 109877 (2021). https://doi.org/10.1016/j.vacuum.2020.109877
82. K.K. Cui, T. Fu, Y.Y. Zhang, J. Wang, H.B. Mao, T.B. Tan, Microstructure and mechanical properties of $CaAl_{12}O_{19}$ reinforced Al_2O_3-Cr_2O_3 composites. J. Eur. Ceram. Soc. **41**(15), 7935–7945 (2021). https://doi.org/10.1016/j.jeurceramsoc.2021.08.024
83. Y.Q. Qiao, J.P. Kong, Q. Li, X.P. Guo, Comparison of two kinds of Si–B–Y co-deposition coatings on an Nb-Ti-Si based alloy by pack cementation method. Surf. Coat. Technol. **327**, 93–100 (2017). https://doi.org/10.1016/j.surfcoat.2017.07.013
84. T. Fu, K.K. Cui, Y.Y. Zhang, J. Wang, F.Q. Shen, L.H. Yu, J.M. Qie, X. Zhang, Oxidation protection of tungsten alloys for nuclear fusion applications: a comprehensive review. J. Alloy. Compd. **884**, 161057 (2021). https://doi.org/10.1016/j.jallcom.2021.161057
85. Y. Zhang, L. Yu, T. Fu, J. Wang, F. Shen, K. Cui, H, Wang, Microstructure and oxidation resistance of Si-MoSi2 ceramic coating on TZM (Mo-0.5 Ti-0.1 Zr-0.02 C) alloy at 1500° C. Surf. Coat. Technol. **431**, 128037 (2022). https://doi.org/10.1016/j.surfcoat.2021.128037
86. K. Cui, Y. Zhang, T. Fu, J. Wang, X. Zhang, Toughening mechanism of mullite matrix composites: a review. Coatings **10**(7), 672 (2020). https://doi.org/10.3390/coatings10070672
87. M. Sankar, V.S. Prasad, R.G. Baligidad, M.Z. Alam, D.K. Das, A.A. Gokhale, Microstructure, oxidation resistance and tensile properties of silicide coated Nb-alloy C-103. Mater. Sci. Eng. A **645**, 339–346 (2015). https://doi.org/10.1016/j.msea.2015.07.063